RSC Advances

This is an *Accepted Manuscript*, which has been through the Royal Society of Chemistry peer review process and has been accepted for publication.

Accepted Manuscripts are published online shortly after acceptance, before technical editing, formatting and proof reading. Using this free service, authors can make their results available to the community, in citable form, before we publish the edited article. This *Accepted Manuscript* will be replaced by the edited, formatted and paginated article as soon as this is available.

You can find more information about *Accepted Manuscripts* in the Information for Authors.

Please note that technical editing may introduce minor changes to the text and/or graphics, which may alter content. The journal's standard Terms & Conditions and the Ethical guidelines still apply. In no event shall the Royal Society of Chemistry be held responsible for any errors or omissions in this *Accepted Manuscript* or any consequences arising from the use of any information it contains.

ROYAL SOCIETY OF CHEMISTRY

www.rsc.org/advances

Please do not adjust margins

Journal Name

ARTICLE

A novel and anti-agglomerating Ni@yolk-ZrO_2 structure with sub-10nm Ni core for high performance steam reforming of methane

Received 00th January 20xx,
Accepted 00th January 20xx

DOI: 10.1039/x0xx00000x

www.rsc.org/

Zi-Yian Lim,[a,b] Chunzheng Wu,[a] Wei Guo Wang,[a] Kwang-Leong Choy,[c] and Hongfeng Yin[a]

Steam reforming of methane is a versatile technology for hydrogen production in oil refinery and fuel cell applications. Using natural gas is a promising method to produce rich-hydrogen gas. Ni@yolk-ZrO_2 catalyst is used to study steam reforming of methane under various GHSVs, steam-to-carbon (S/C) ratio, and its recyclability. The catalyst was characterized using a combination of XRD, TEM, AAS, TPR, TPH, TGA, BET, XPS, and Raman techniques. The catalyst is evaluated on time stream and identify its anti-agglomeration property and coking mechanism . From the characterization of TEM and XPS establish the information of Ni particles mobility in the catalyst, which active metal particle size was controlled under the yolk-shell structure framework. Furthermore, the results from TGA,TPH, and Raman analysis of the used Ni@yolk-ZrO_2 catalyst showed the characteristic of inhibiting formation of highly ordered carbon structure.

1. Introduction

The steam reforming of methane is a well established industrial process for the production of hydrogen and synthetic gas.[1, 2] Ni-based catalysts are commonly used in industrial reforming reactions due to their low cost and high activity. However, these catalysts deactivate fast due to sintering[5] and coke deposition[7]. Therefore, excess steam (S/C > 3) is introduced in the feedstock to prevent coke deposition. The excess steam favour water gas shift reaction that produce higher amount of hydrogen gas. However, steam at high temperature can be corrosive and invasive towards the catalysts. It also leads to deactivation of the catalyst due to oxidation of Ni species.[8] Therefore, in order to prevent sintering and coke deposition while maintaining the catalyst integrity were the biggest challenges in the steam reforming process.

Several studies discuss enhancing the stability of Ni-based catalyst for the reforming reaction. Promotes such as alkaline earth (MgO or CaO) are often used to lower the coke formation and provide higher stability against sintering.[9] However, the addition of these promoters obstructs the reduction of NiO leading to less active metals involve in the reactions. It has been observed that promotion with K or Ca increases the formations of $NiAl_2O_4$ phase, whereby Ni was substituted in the inert spinel structure and became inactive.[10] It was reported that adding tolerable alkaline metal oxide suppressed the coke deposition in the reforming reaction. Hence, it is crucial that the modification of Ni-based catalysts do not compromise the activity.

It is evident that the reducible support (e.g. CeO_2) provides better stability and coke resistance in comparison with non-reducible supports.[11, 12] As they have direct advantage of oxygen storage capacity that significantly reduce the coke formation on the catalyst surface.[13] Ceria and ceria-doped supports are well known for their reversible exchange of lattice oxygen during reaction.[14] However, CeO_2 support is vulnerable to sintering and loses its oxygen storage capacity (OSC) at high temperatures (e.g. above 500°C).[15] Also, CeO_2 could fully cover the active metal during the redox reactions due to their amorphous feature which lead to deactivation.[16]

The activity of the catalyst often depends on the size and extent of metal dispersion.[17, 18] Small particles increase metal dispersion and also provide more active site (steps/kinks) on the surface.[19] The energy barrier for methane dissociation is much lower at step sites. Therefore, the rate of reaction increases with smaller particles as they consisted of highly concentrated active phase of step sites.[20] Besides, small particles below a critical size have also been reported to be more resistant to coke formation.[21] The highly dispersed active metal particles also tend to minimize surface energy by strongly interact with the support and reduce sintering occurrence. Hence, Ni with good particle size homogeneity and metal support interaction are essential for a highly stable catalyst.

The preparation method often influences the structure and morphology of the catalyst. Recently, a method of embedding the active metal nanoparticles in inorganic cavities shows

[a] Ningbo Institute of Material Technology and Engineering, 519 Zhuangshi Road, Zhenhai District, Ningbo 315201, China. E-mail: yinhf@nimte.ac.cn
[b] University of Nottingham, Ningbo China, 199 Taikang East Road, University Park, Ningbo 315100, China. E-mail: zx08427@nottingham.edu.cn
[c] UCL Institute for Materials Discovery, University College London, Kathleen Lonsdale Building, Gower Place, London, WC1E6BT, United Kingdom. Email: k.choy@ucl.ac.uk. Tel: +44(0) 207679 3855
† Footnotes relating to the title and/or authors should appear here.
Electronic Supplementary Information (ESI) available: [details of any supplementary information available should be included here]. See DOI: 10.1039/x0xx00000x

RSC Advances Accepted Manuscript

promising application in preventing sintering of active metal.[22] Among these materials, highly defined nanostructure of core-shell and yolk-shell structure have demonstrated excellent properties in various applications, for example, Au-Ni@SiO_2 for hydrolytic dehydrogenation of ammonia borane,[23] metal@TiO_2 yolk-shell nanostructures for photocatalytic dye degradation[24] and Au@ZrO_2 for CO oxidation.[25] Of particular interest is Au@ZrO_2 yolk-shell nanostructure. This is because it has great potential to be developed for highly stable and ease of gaseous exchange in catalytic applications. In addition, the structure is easy to be modified such as its porosity through modification of the shell to further improve its catalytic performance.[26] In this paper, we report a Ni@yolk-ZrO_2 catalyst synthesized via double template emulsion method which shows substantial long term high activity and successfully performed for multiple cycles without deterioration under operation mode of steam reforming of methane at S/C molar ratio of 2.5.

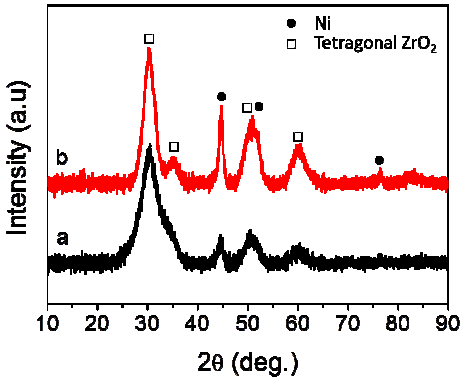

Fig 2. XRD of Ni@yolk-ZrO_2 (a) and impregnated Ni/ZrO_2 (b), both reduced at 650°C for 3 hours.

2. Experimental

2.1 Synthesis and characterization

Synthesis of Ni colloids and Ni@SiO_2. The synthesis of Ni@SiO_2 colloids was carried out by reverse micelle approach. Typically, 3ml of aqueous 0.25M $NiCl_2$ and 11.5ml of Brij L4 (Sigma-Aldrich) were mixed with 40ml of n-octane in a 250ml 3-neck round bottom flask at 30°C under N_2 atmosphere protection. The mixture was stirred for 10 min. 1ml of 3.172M ice-cooled $NaBH_4$ solution was drop quickly into the flask. Immediately, a clear solution would turn into pitch black and bubbles were generated. After 5 minutes of N_2 purge, the inlet and outlet were sealed. Subsequently the solution was stirred for 12 hours to form stable Ni colloids. The SiO_2 coating achieved by subsequently adding 50ml of n-octane, 2.4ml Brij L4, 1.2ml ammonia (26%-28%), 2ml of TEOS into the solution and kept stirring for 3 hours. After 3 hours, additional 2ml of TEOS was added and stirred for another 5 hours. The Ni@SiO_2 colloids was obtained after centrifuge and washed with acetone and ethanol, then re-dispersed into 40ml of ethanol.

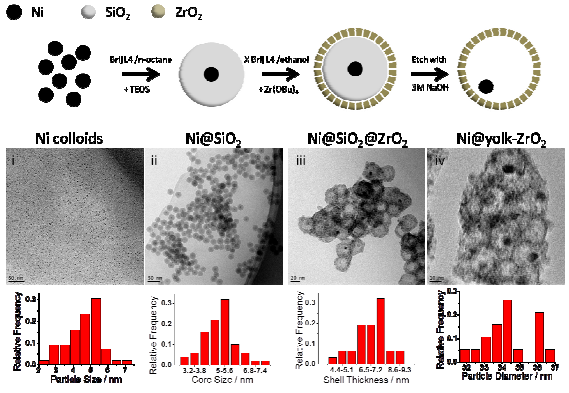

Fig 1. A schematic diagram of the synthetic route of Ni@yolk-ZrO_2 catalyst, and the associated TEM of the structures and core size distributions.

Synthesis of Ni@SiO_2@ZrO_2. 35ml of dispersed Ni@SiO_2 colloids in ethanol was used for the subsequent synthesis by mixing with 0.6ml Brij L4, 0.6ml H_2O in 220ml of ethanol and stirred for 30 minutes. Then, 2ml of $Zr(OBu)_4$ was added and vigorously stirred for 8hours at 30°C. The colloids were washed with ethanol twice and re-dispersed into 40ml deionized water with 0.001M $NaBH_4$ and aged for 3 days. The powder was collected and dried under 105°C for 3 hours and calcined at 750°C (2°C/min) for 3 hours.

Synthesis of Ni@yolk-ZrO_2. The calcined powder was dispersed into 40ml of 3M NaOH solution for 48 hours under stirring. The colloids were washed with deionized water several times. After drying at 105°C for 3 hours, the powder was calcined at 550°C. Subsequently, the obtained powder was reduced under H_2 atmosphere at 650°C for 3 hours.

Synthesis of Ni/ZrO_2. 1g of commercially made ZrO_2 powder (TOSOH) was impregnated with 50ml of 0.017M NiCl and stirred under room temperature. After 6 hours, the obtained sol was dried at 100 °C for 3 hours and subsequently calcined at 750 °C for 3 hours, followed by reduction under H_2 atmosphere at 650°C for 3 hours.

X-ray diffraction patterns were recorded using Bruker D8 Advance with Cu-Kα radiation (λ = 1.5418 Å) in the 2θ range of 10°-90°. Transmission electron microscopy (TEM), model JEM 2100 was used to study the morphology and microstructure of the catalyst. The TEM specimens were prepared by dropping a trace amount of the sample dispersed in ethanol on a carbon coated copper grid (300 mesh). The BET surface area measurement was carried out using a Micrometrics ASAP 2020M apparatus at 77 K. Prior to the measurement, the sample was degassed at 300°C for 5 h under vacuum. Temperature-programmed reduction (FINESORB3010E, Zhejiang Fintec Co.) was performed to determine the nickel species and its reducibility for each catalyst. Typically, catalyst was filled into a U-shape quartz tube and held by quartz wool. Prior to reduction, the sample was treated with pure Ar for 30 min at 300°C to remove any impurities. The temperature was

RSC Advances Accepted Manuscript

This journal is © The Royal Society of Chemistry 20xx

then cooled down to room temperature. 10%H_2/Ar (25mlmin^{-1}) was introduced, and the temperature was increased from room temperature to 800°C with a heating rate of 5°Cmin^{-1}. A temperature programmed hydrogenation was used to identify the carbon species of the used catalyst. Typically, used catalyst (30mg) was loaded into a U-shape quartz tube and held by a quartz wool. Prior to hydrogenation, the sample was treated under pure Ar for 3 h at 100°C and cooled down to room temperature. Then, a mixture of 10%H_2/Ar (25mlmin^{-1}) was introduced into the sample. After 2 hours, the temperature was increased to 900°C with a heating rate of 5°Cmin^{-1}. X-ray photoelectron spectroscopy (XPS) spectra were recorded on a Shimadzu Axis Ultradld spectroscope (Japan) using the monochromatized Al Kα radiation resource at room temperature and under a vacuum of 10^{-7} Pa (10^{-9} Torr). The starting angel of the photoelectron was set at 90°. The spectrum was calibrated with a C 1s spectrum of 248.8 eV. Raman spectra were collected using a Renishaw inVia Reflex (λ=532nm) and a CCD detector. The spectrum acquisition consisted of 10 accumulations for 30 s. The spectra were recorded at ambient temperature. Thermogravimetric analysis (TGA) was conducted using Perkin-Elmer Pyris Diamond TGA equipment. The used catalysts were preheated under a flow of nitrogen (100mlmin^{-1}) for 30 min. Then the samples were heated in air (100mlmin^{-1}) by raising the temperature from room temperature to 1000°C at a rate of 10Cmin^{-1}.

2.2 Catalytic evaluation

Steam reforming of methane was studied in a fixed bed quartz reactor (12mm ID) under atmospheric pressure. The reactor was equipped with a pre-heater, a syringe pump, a cold condenser and a gas flow meter. 100mg of catalyst diluted with filled quartz sand of 2cm length was used. The quartz reactor loaded with catalyst was heated in an electric furnace and the temperature of the bed was controlled by a K-type thermocouple positioned at the center of the catalyst bed. Prior to the test, the catalyst was reduced *in situ* 650°C with 10%H_2/Ar mixture (50 mlmin^{-1}) for 3 h. A reaction mixture of H_2O and CH_4 (Steam to carbon molar ratio of 2.5:1) without dilution was fed using a gas hourly space velocity (GHSV) of 50,400 ml$g_{cat}^{-1}h^{-1}$. The effluent gases were analyzed by an on-line gas chromatography (INESA Scientific Instrument Co.Ltd, GC-122) equipped with a packed column (TDX-01) and a TCD detector. A cold trap was placed before the TCD to remove moisture in the gas products. The peak area normalization method was used for quantitative analysis of effluent gaseous[27, 28]. The CH_4 conversion and CO selectivity were calculated using equations (1) and (2) as follows:

$$X_{CH_4}(\%) = \frac{[CO] + [CO_2]}{[CO] + [CO_2] + [CH_4]} \times 100 \quad (1)$$

$$CO\ selectivity\ (\%) = \frac{[CO]}{[CO] + [CO_2]} \times 100 \quad (2)$$

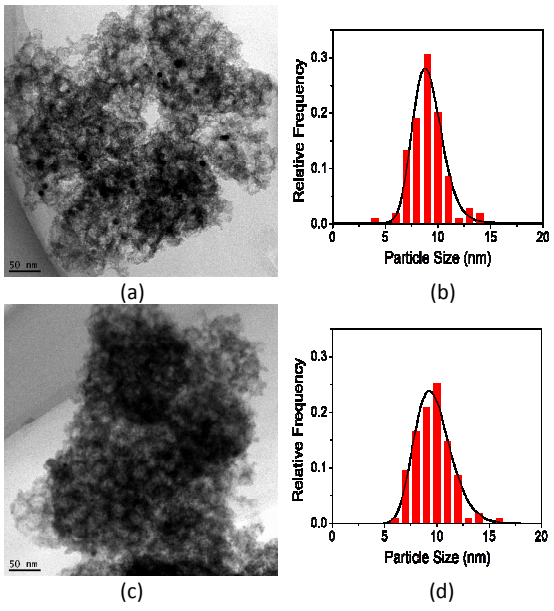

Fig 3. TEM images of Ni@yolk-ZrO_2 before (a) and after 48 h (c) steam reforming test and their Ni core particle size distribution (b) and (d) respectively.

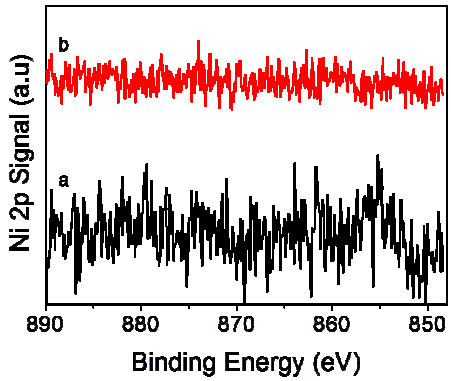

Fig 4. XPS selected scan of Ni 2p signal of Ni@yolk-ZrO_2 before (a) and after (b) test.

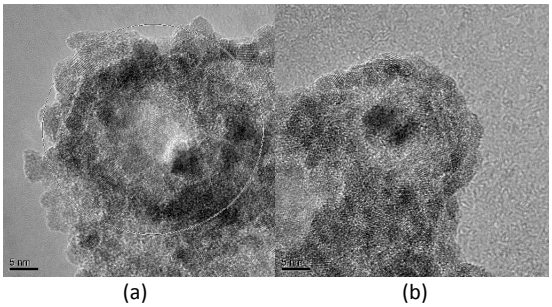

Fig 5. HRTEM images of Ni@yolk-ZrO_2 before (a) and after 48 h (b) steam reforming test.

RSC Advances Accepted Manuscript

Table 1. XPS analysis of the relative mass concentration of Ni@yolk-ZrO_2 and impregnated Ni/ZrO_2 catalysts before and after steam reforming test

Catalysts	Ni 2p (%)	O 1s (%)	Zr 3d (%)	Si 2p (%)
Ni@yolk-ZrO_2-before	2.78	36.3	45.5	15.41
Ni@yolk-ZrO_2-after	0	31.13	40.02	22.69
Ni/ZrO_2-before	7.88	21.57	70.54	-
Ni/ZrO_2-after	7.49	36.13	56.38	-

3. Results and discussion

3.1 Structural studies

XRD patterns of the catalyst are shown in Fig.2. The Ni@yolk-ZrO catalyst shows a low crystallinity of Ni metal compared to impregnated Ni/ZrO_2 catalyst. The catalysts showed the characteristic peaks of tetragonal ZrO_2 and Ni metal. The peaks observed at 2θ = 44.5°, 51.8°, and 76.4° can be assigned to the (111), (200), (220) planes of Ni metal, respectively. The average crystallite size of Ni was determined by the peak broadening of the (111) reflection in the XRD patterns, using the Scherrer formula, and was found to be 3.6nm and 213.6nm respectively, for the Ni@yolk-ZrO_2 and impregnated Ni/ZrO_2 catalysts. Furthermore, Ni@yolk-ZrO_2 has a relatively broaden peak of tetragonal phase ZrO_2 at 30.5° (111) as compared to impregnated Ni/ZrO_2 and their crystallite size are 1.4nm and 42.4nm, respectively. This shows that Ni particles were highly disperse in the nano-framework of tetragonal phase ZrO_2.

The TEM micrographs of Ni@yolk-ZrO_2 catalyst before and after steam reforming test are shown in Fig. 3 and Fig. 5. Before reforming test, the Ni particles are uniformly distributed over the ZrO_2 hollow shell and no apparent aggregation of particles was observed. The average particle size of Ni is about 8.9nm. After 48 h on steam reforming of methane, the particle size increased to circa. 9.6nm. The crystallite size of Ni and the average Ni particle size from TEM observation was 8.9nm. Fig.4 shows the XPS Ni 2p peak of freshly reduced Ni@yolk-ZrO_2 with detectable Ni particles over the catalyst surface, in contrast, the used-catalyst showed almost the non-existence of Ni particles over the catalyst surface. From the XPS depth analysis,[29, 30] Ni particles have been detected partly in the matrix of ZrO_2 hollow shell before testing and inside the hollow shell after steam reforming of methane testing. In addition, the Ni mass concentration is diminished after the reforming testing of Ni@yolk-ZrO_2 catalyst while the impregnated Ni/ZrO_2 remained the same. This result indicated Ni particles have been moving toward inside the ZrO_2 hollow shell during catalytic testing.

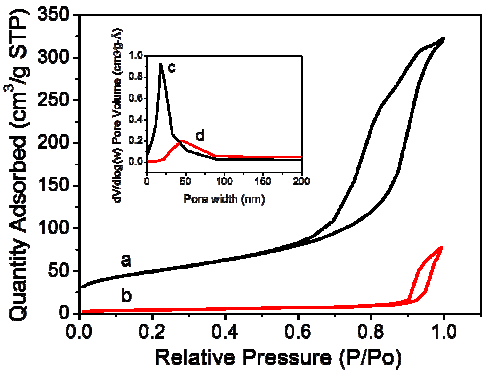

Fig 6. BET isotherm of Ni@yolk-ZrO_2 (a) and Ni/ZrO_2 (b). Inset: Pore size distribution of Ni@yolk-ZrO_2 (c) and Ni/ZrO_2 (d)

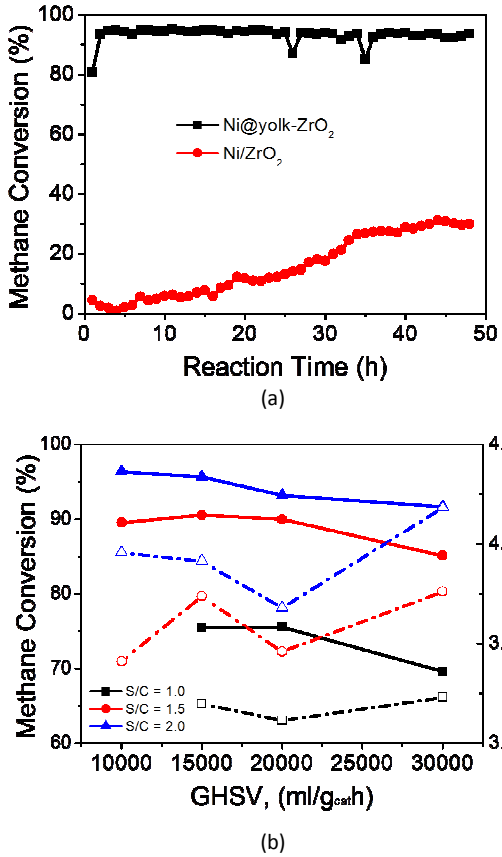

Fig 7. Catalytic steam reforming of methane on Ni@yolk-ZrO_2 and Ni/ZrO_2 catalyst (a). Catalytic performance and H_2/CO ratio under various GHSVs and S/C ratio on Ni@yolk-ZrO_2 catalyst (b).

RSC Advances Accepted Manuscript

This journal is © The Royal Society of Chemistry 20xx

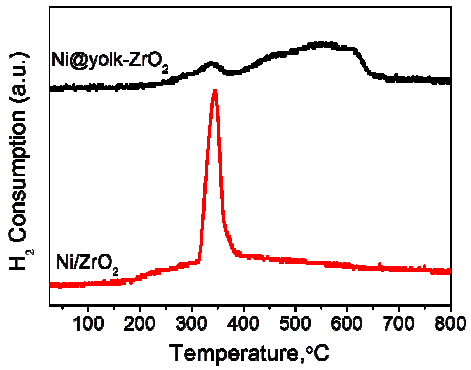

Fig 8. Temperature-programmed reduction of the catalysts.

The BET isotherm graph (Fig. 6) showed Ni@yolk-ZrO_2 has Type-IV isotherm characteristic and hysteresis loop of category H3. It has high amount micropore (P/Po < 0.1) as compared to impregnated Ni/ZrO_2. It also has the characteristic of multilayer adsorption before the onset of capillary condensation. The slope of the multilayer adsorption suggesting slit-shaped pore might present between the nano-size ZrO_2 grains in the shell which would allow gaseous exchange to occur during reactions. XRD patterns of Ni@yolk-ZrO_2 showed broadening peaks of tetragonal phase of ZrO_2, implicating the occurrence of multilayer adsorption of the shell is indeed promoting the high degree of reactants and products exchange. Besides, the capillary condensation is the void space between the Ni core and ZrO_2 shell with 18nm pore. The void space would allow active Ni particle to move freely around but was inhibited to move outside the shell attributed to the presence of the slit-shaped framework of the ZrO_2 shell. Such characteristic is advantageous to significantly reduce active Ni particles from agglomerating with each other and limiting their particle growth.

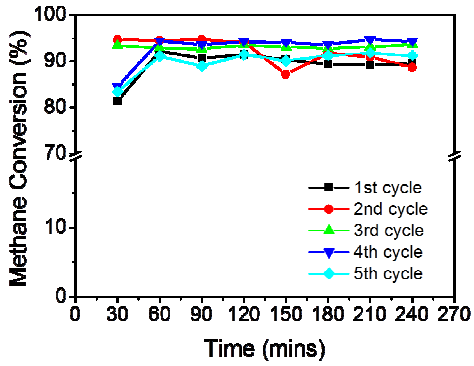

(a)

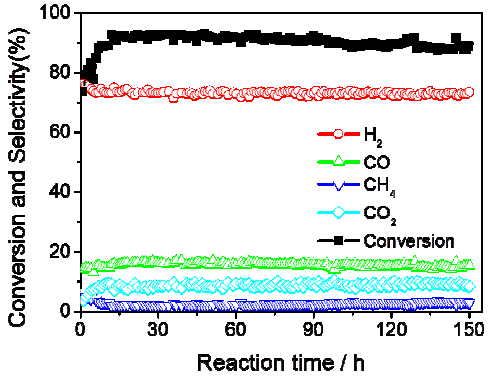

(b)

Fig 9. Reusability of Ni@yolk-ZrO_2 on steam reforming of methane (a) and 150 hours durability test on Ni@yolk-ZrO_2 catalyst (b).

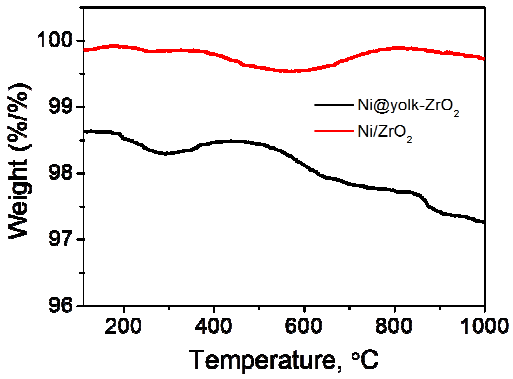

(a)

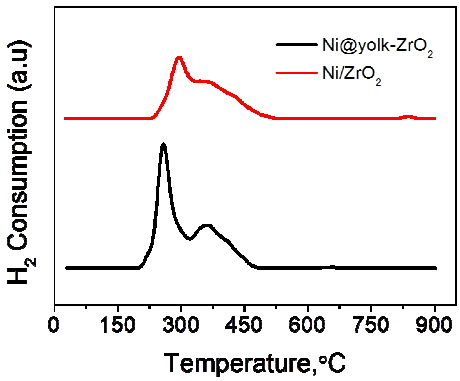

(b)

Fig 10. TGA analysis (a) and TPH analysis (b) of used catalysts under condition S/C = 2.5.

3.2 Catalytic evaluation

The catalytic steam reforming of methane of yolk-shell and impregnated catalysts were studied at GHSV of 50,400 ml/$g_{cat}^{-1}h^{-1}$ and S/C=2.5 at 750°C, and the results are shown in Fig. 7a.

RSC Advances Accepted Manuscript

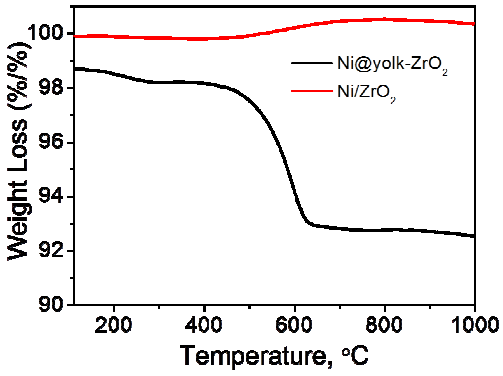

(a)

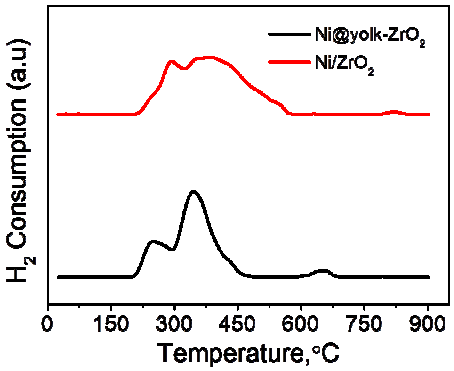

(b)

Fig 11. TGA analysis (a) and TPH analysis (b) of used catalysts under condition S/C = 1.

The methane conversion on Ni@yolk-ZrO_2 catalyst increases with time on steam reforming. Initially reaction time, and then the methane conversion kept at 90% with time on stream. In comparison with impregnated Ni/ZrO_2, the methane conversion is low and increases slowly with time on stream and reached a plateau of 30%. For Ni@yolk-ZrO_2 catalyst, activity maintained with time on stream that may be contributed to the homogenously distributed active Ni particles. In addition, the TPR testing (Fig. 8) shows that less free NiO species formed in the Ni@yolk-ZrO_2 catalyst as compared to impregnated Ni/ZrO_2 which may stabilize the Ni particle size and influence the catalytic activity.

Analysing the effect of the reaction temperature on the catalytic performance of Ni@yolk-ZrO_2, a temperature of 750°C was kept to study the effect of GHSVs. The purpose of this study is to optimize the possibility of reactants that could

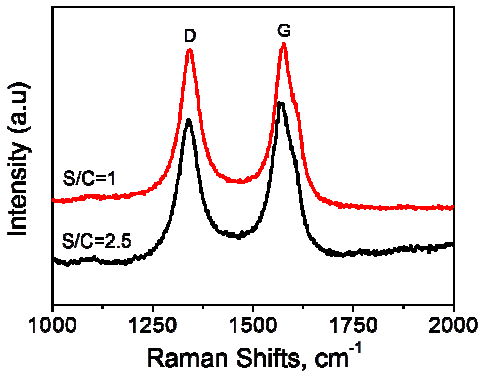

Fig 12. Raman spectra of used Ni@yolk-ZrO_2 catalyst.

be process into synthesis gas. Moreover, steam reforming is an energy consuming process and it is necessary to reduce the process cost. Hence, the methane content in the feed was changed, and the results are depicted in Fig. 7b. As the GHSVs increased, the methane conversion decreased for all S/C conditions. The catalyst performance maintained up to 85% or above of methane conversion (for S/C = 1.5 and S/C = 2), when S/C = 1, the methane conversion was maintained up to 70% or above. Also, it can be observed that the H_2/CO ratio for all conditions is particularly low at GHSV of 20,000 $ml g_{cat}^{-1} h^{-1}$ and a higher content of CO was produced at this operating condition.

The same catalyst was subjected to recyclability test of steam reforming of methane under S/C = 2.5. The catalyst was tested for 4hours, oxidizes in air at 500°C for 1 hour, reduced at the same temperature for 1 hour, and repeated these cycles for 5 times. The catalyst exhibited a methane conversion of 90% which is almost constant along 5 reaction cycles (Fig. 9a). Also, the catalyst was tested on stream and remained active and continuously producing synthetic gas for 150 hours (Fig. 9b). It is remarkable that the catalyst performance of the Ni@yolk-ZrO_2 exhibiting superior catalytic effect in steam reforming of methane.

3.3 Coking mechanism

Coke formation during steam reforming of methane causes the deactivation of catalysts. The most possible reactions[31] leading to the carbon formation in steam reforming of methane were:

$$2CO \rightarrow CO_2 + C \quad (3)$$

$$CH_4 \rightarrow 2H_2 + C \quad (4)$$

RSC Advances Accepted Manuscript

This journal is © The Royal Society of Chemistry 20xx

Please do not adjust margins

Table 2. Selected results of core shell or yolk-shell structured catalysts in reforming of methane

Catalyst	Ni wt%	GHSV	Conditions	Temperature	X_{CH4}
Ni@yolk-ZrO_2	5.08	50400	SRM (S/C=2.5)	750	93.0
Ni@SiO_2 yolk-shell[3]	89	100000	SRM (S/C=4)	700	90.0
10 wt% Ni/$MgAl_2O_4$[4]	10	54000	SRM (S/C=2)	750	97.2
NiO-350@meso-SiO_2	54.8	72000	POM	750	93.0
Ni–Yolk@Ni@SiO_2[6]	18.6	36000	DRM	800	90.0

Equation (3) and (4) were the Boudouard reaction and methane decomposition which were preliminary formation of carbon nanotubes and graphites.[32] Therefore, it is essential to determine the carbon species formed in the Ni@yolk-ZrO_2 catalyst as compared to impregnated Ni/ZrO_2. Fig. 10a represents the TGA of both tested catalyst. It is noticed that Ni@yolk-ZrO_2 has higher weight loss than Ni/ZrO_2 with carbon deposition rate of 1.15 $mg_c g_{cat}^{-1} h^{-1}$ after 48 hours. This might be due to methane dissociation[33] is higher for smaller Ni particles size of Ni@yolk-ZrO_2 than Ni/ZrO_2; hence a higher weight loss would occur on the Ni@yolk-ZrO_2 catalyst. In order to understand the carbon species formed in the catalysts, it was subjected to TPH after steam reforming of methane. As identified in Fig. 10b that the surface carbon species on Ni@yolk-ZrO_2 is weak than Ni/ZrO_2 and the first peaks of carbon species are at 260°C and 293°C respectively. The first peak might be amorphous carbon (α-carbon) on the nickel sites. Second and third peaks would be whisker carbon (β-carbon) or graphitic carbon (γ-carbon) exists in the catalyst. It can be seen that Ni/ZrO_2 has a broad shoulder peak at 360°C and a small peak at 835°C. The impregnated Ni/ZrO_2 catalyst has higher order carbon species formed during the steam reforming of methane as compared to Ni@yolk-ZrO_2 with only α and β carbon. The main carbon deposited in Ni@yolk-ZrO_2 was amorphous carbon due to high density of kinks existing in small Ni particles size and this amorphous carbon was readily to be reacted with steam. Furthermore, both of the catalyst were carried out under S/C =1 with the same GHSV of 50400 $ml g_{cat}^{-1} h^{-1}$ for 12 h in order to understand the carbon species formation in Ni@yolk-ZrO_2. From Fig. 11, the weight loss is significantly higher with 5% carbon (3.29 $mg_c g_{cat}^{-1} h^{-1}$) was deposited. However, from the TPH analysis, the first peak diminished and second peak was intensified. As for the third peak which occurred at 650°C indicating a higher ordered carbon has formed, but the temperature lies lower than impregnated Ni/ZrO_2 catalyst. This phenomenon suggesting yolk-shell structure inhibiting the formation of highly ordered carbon in Ni@yolk-ZrO_2 catalyst. Further validation of Raman (Fig. 12) of the tested catalysts (S/C =2.5 and S/C =1) showed the presence of the spectra of D band and G band of carbon has the relative intensity ratio I_D/I_G of 0.94 and 0.96. It demonstrates the ZrO_2 shell has inhibited the continuous growth of whisker carbon or graphitic carbon from Ni particle. It can be concluded that Ni@yolk-ZrO_2 exhibiting the capability of inhibiting the formation of higher ordered carbon during steam reforming of methane.

Conclusions

Ni@yolk-ZrO_2 nanoparticles with sub-10nm Ni cores were synthesized via a double template method and evaluated for steam reforming of methane. The effect of introducing ZrO_2 shell for steam reforming of methane was discused for the first time. It was found that the active Ni particles agglomerating behaviour was controlled by the ZrO_2 shell and showed high activity on steam reforming of methane at 750°C. XPS analysis showed Ni particles was confined in the ZrO_2 shell. The ZrO_2 shell has not only prevented the mobility of the Ni particles but also limited their growth. Raman and TPH analysis hav provided the evident that ZrO_2 shell hindered the severe sintering of active Ni particles and continuously providing high catalytic activity in steam reforming of methane. In addition, the yolk-shell structure has the capability to inhibit the formation of highly ordered carbon deposit on the catalyst surface attributed to ZrO_2 shell isolating highly dispersed active Ni particles. After 150 hours of reaction, Ni@yolk-ZrO_2 nanoparticles preserved their structures and remained active. It is remarkable to develop and comprehend such properties of the catalyst which is possible to be extended to other active metals and high temperature reactions.

Acknowledgements

This work is supported by the National Basic Research Program of China (2013CB934800), the Innovation Team Foundation (2014B81004) from the Ningbo Science and Technology Bureau, and Zhejiang Province Natural Science Foundation (LY15B030005). ZYL acknowledged the scholarship awarded by the University of Nottingham, Ningbo China.

Notes and references

1. B. Höhlein, S. von Andrian, T. Grube and R. Menzer, *Journal of Power Sources*, 2000, **86**, 243-249.
2. A. P. Simpson and A. E. Lutz, *International Journal of Hydrogen Energy*, 2007, **32**, 4811-4820.
3. J. C. Park, J. U. Bang, J. Lee, C. H. Ko and H. Song, *Journal of Materials Chemistry*, 2010, **20**, 1239-1246.
4. H.-W. Kim, K.-M. Kang, H.-Y. Kwak and J. H. Kim, *Chemical Engineering Journal*, 2011, **168**, 775-783.

RSC Advances Accepted Manuscript

5. J. Sehested, A. Carlsson, T. V. W. Janssens, P. L. Hansen and A. K. Datye, *Journal of Catalysis*, 2001, **197**, 200-209.
6. Z. Li, L. Mo, Y. Kathiraser and S. Kawi, *ACS Catalysis*, 2014, **4**, 1526-1536.
7. I. H. Son, S. J. Lee, A. Soon, H.-S. Roh and H. Lee, *Applied Catalysis B: Environmental*, 2013, **134–135**, 103-109.
8. J. H. Jeong, J. W. Lee, D. J. Seo, Y. Seo, W. L. Yoon, D. K. Lee and D. H. Kim, *Applied Catalysis A: General*, 2006, **302**, 151-156.
9. L. Xiancai, W. Min, L. Zhihua and H. Fei, *Applied Catalysis A: General*, 2005, **290**, 81-86.
10. T. Osaki and T. Mori, *Journal of Catalysis*, 2001, **204**, 89-97.
11. N. Laosiripojana and S. Assabumrungrat, *Applied Catalysis A: General*, 2005, **290**, 200-211.
12. J. Gao, J. Guo, D. Liang, Z. Hou, J. Fei and X. Zheng, *International Journal of Hydrogen Energy*, 2008, **33**, 5493-5500.
13. R. Craciun, W. Daniell and H. Knözinger, *Applied Catalysis A: General*, 2002, **230**, 153-168.
14. R. B. Duarte, M. Nachtegaal, J. M. C. Bueno and J. A. van Bokhoven, *Journal of Catalysis*, 2012, **296**, 86-98.
15. J.-G. Li, T. Ikegami and T. Mori, *Acta Materialia*, 2004, **52**, 2221-2228.
16. X. Wang and R. J. Gorte, *Applied Catalysis A: General*, 2002, **224**, 209-218.
17. J. Wei and E. Iglesia, *Journal of Catalysis*, 2004, **225**, 116-127.
18. G. Jones, J. G. Jakobsen, S. S. Shim, J. Kleis, M. P. Andersson, J. Rossmeisl, F. Abild-Pedersen, T. Bligaard, S. Helveg, B. Hinnemann, J. R. Rostrup-Nielsen, I. Chorkendorff, J. Sehested and J. K. Nørskov, *Journal of Catalysis*, 2008, **259**, 147-160.
19. K. O. Christensen, D. Chen, R. Lødeng and A. Holmen, *Applied Catalysis A: General*, 2006, **314**, 9-22.
20. D. A. J. M. Ligthart, R. A. van Santen and E. J. M. Hensen, *Journal of Catalysis*, 2011, **280**, 206-220.
21. J. Sehested, *Catalysis Today*, 2006, **111**, 103-110.
22. M. Pérez-Lorenzo, B. Vaz, V. Salgueiriño and M. A. Correa-Duarte, *Chemistry – A European Journal*, 2013, **19**, 12196-12211.
23. H.-L. Jiang, T. Umegaki, T. Akita, X.-B. Zhang, M. Haruta and Q. Xu, *Chemistry – A European Journal*, 2010, **16**, 3132-3137.
24. J. B. Joo, M. Dahl, N. Li, F. Zaera and Y. Yin, *Energy & Environmental Science*, 2013, **6**, 2082-2092.
25. P. M. Arnal, M. Comotti and F. Schüth, *Angewandte Chemie*, 2006, **118**, 8404-8407.
26. P. M. Arnal, C. Weidenthaler and F. Schüth, *Chemistry of Materials*, 2006, **18**, 2733-2739.
27. Y. J. Wu, J. C. Santos, P. Li, J. G. Yu, A. F. Cunha and A. E. Rodrigues, *The Canadian Journal of Chemical Engineering*, 2014, **92**, 116-130.
28. Q. Jing, H. Lou, L. Mo and X. Zheng, *Energy Conversion and Management*, 2006, **47**, 459-469.
29. M. J. Ariza, E. Rodríguez-Castellón, M. Muñoz and J. Benavente, *Surface and Interface Analysis*, 2002, **34**, 637-641.
30. C. Y. Tang, Y.-N. Kwon and J. O. Leckie, *Journal of Membrane Science*, 2007, **287**, 146-156.
31. S. Sokolov, E. V. Kondratenko, M.-M. Pohl, A. Barkschat and U. Rodemerck, *Applied Catalysis B: Environmental*, 2012, **113–114**, 19-30.
32. A. F. Cunha, J. J. M. Órfão and J. L. Figueiredo, *International Journal of Hydrogen Energy*, 2009, **34**, 4763-4772.
33. A. F. Cunha, J. J. M. Órfão and J. L. Figueiredo, *Applied Catalysis A: General*, 2008, **348**, 103-112.

RSC Advances Accepted Manuscript

This journal is © The Royal Society of Chemistry 20xx